Research Article | Vol. 4, No. 2 / 15 February 2021 / OSA Continuum 385
OSA CONTINUUM

Design of a high uniform collimation illumination system for near field measurement

YAO DONG,[1,2,3,*] XU MINGFEI,[1,4] LV TAO,[1,3] YAN CHUNHUI,[1,3] MENG LINGTONG,[1,3] AND HUANG WEI[1,4]

[1]Changchun Institute of Optics, Fine Mechanics and Physics, Chinese Academy of Sciences, Changchun 130033, China
[2]University of Chinese Academy of Sciences., Beijing 1000409, China
[3]Key Laboratory of Airborne Optical Imaging and Measurement, Chinese Academy of Sciences, Changchun 130033, China
[4]State Key Laboratory of Applied Optics, Changchun Institute of Optics, Fine Mechanics and Physics, Chinese Academy of Sciences, Changchun, Jilin 130033, China
[*]171502099@qq.com

Abstract: In this paper, focusing on the needs of near-field measurement lighting, a lighting system with high collimation and uniformity is designed, using filament high-heat illuminant as radiation source. The general design idea of dividing the illumination system into "collimating optical cavity" and "homogenizing optical cavity" is put forward. The design process of "collimating optical cavity" is given, and two different structural forms of "homogenizing optical cavity" are analyzed and the design results are given. The lighting effect is obtained by using simulation software, and the established parameters are achieved.

1. Introduction

In the field of precision measurement or precision machining, lighting system plays a vital role. For example, in the microscopic imaging system, there are two different lighting methods: critical lighting and Kohler lighting. At present, the mainstream technical route is Kohler lighting [1–5]. In VLSI processing, the illumination system is located between the laser and the projection objective, which provides the illumination light field with specific intensity distribution for the mask plate, thus ensuring that the mask pattern can be imaged on the silicon wafer surface with high fidelity through the projection objective [6–8]. In the field of 3D measurement of Lambert surface, some scholars have proposed a scaled SFS method under the illumination of near point light source [9]. In the field of laser illumination, because the laser intensity emitted by lasers is mostly Gaussian distribution, and the actual demand is mostly flat top distribution, various technical routes such as aspheric surface shaping, binary optical element shaping, homogeneous light guide rod, optical fiber shaping, etc. [10–14].

The microscopic measurement system has a very small measurement field of view, and the lighting system matched with it is relatively mature [15–18]. However, in some lighting applications, such as wide spectrum illumination measurement experiment, it is required that the illumination light has Large lighting range, wide spectrum range, good collimation characteristics, good uniformity and adequate radiant energy. The combination of these constraints increases the complexity of the lighting system. Therefore, the design of this illumination optical system is a challenging engineering problem worth discussing, and the available lighting cases are rarely reported.

Double telecentric lens keeps consistent magnification in depth of field and has no perspective error, so it plays a vital role in industrial inspection, metrology, lithography and other fields [19][20]. However, because the object telecentric lens often has a short working distance, and the measured object often needs active illumination, the illumination space is often relatively

#414835 https://doi.org/10.1364/OSAC.414835
Journal © 2021 Received 12 Nov 2020; revised 27 Dec 2020; accepted 28 Dec 2020; published 27 Jan 2021

OSA CONTINUUM

narrow, so the illumination system often needs to be designed with the same aperture as the imaging system. The lighting quality has a vital influence on the imaging system. Combined with the characteristics of the measurement system, choosing uniform and vertical lighting is more conducive to improving the measurement quality [20].

Traditional lighting forms mainly include critical lighting and Kohler lighting. The advantage of critical illumination is that the light source is imaged on the object after passing through the condenser, the system structure is simple and the energy utilization rate is high; However, the shortcomings are also obvious: the filament image coincides with the plane of the object, resulting in uneven illumination of the object, which is manifested in the bright part with filament and the dim part without filament, which seriously affects the imaging quality. The schematic diagram of the illumination system is shown in Fig. 1. Professor Kohler put forward a new illumination method in 1893. The light emitted by the light source is projected to the aperture stop through the collecting lens. The position of the aperture stop is conjugate with that of the light source. The distance from the aperture stop to the main plane of the condensing lens set is the focal length of the condensing lens set. Therefore, the image point of the light source is nearly collimated and uniformly emitted after passing through the condensing lens set. The schematic diagram of the illumination system is shown in Fig. 2.

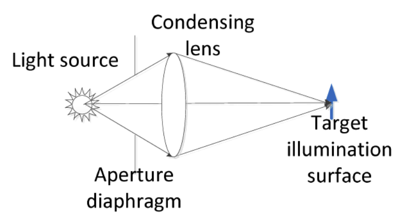

Fig. 1. Schematic diagram of critical lighting

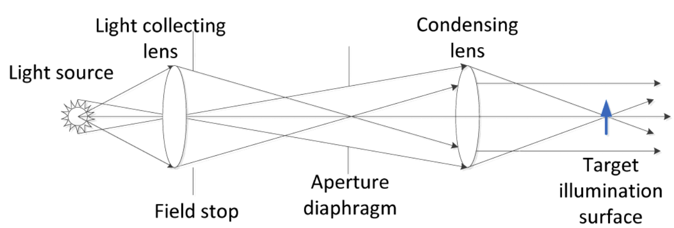

Fig. 2. Schematic diagram of Kohler lighting structure

Although LED is a new type of light source, it has the advantages of high energy efficiency, small size and long life, but its single power is low, the spectral range is relatively narrow, and the flatness of the spectrum is not ideal. Therefore, filament light source has many advantages such as high power, wide and relatively flat spectral range, simple radiation energy modulation and so on. Filament light source has relatively high radiation energy, but its energy radiation direction is spherical, and the energy radiation in all directions is uneven. These characteristics make it difficult to obtain "good collimation characteristics, good uniformity and high illumination effect of radiation energy".

The purpose of the optical system design in this paper is to assist the wide spectrum illumination telecentric measurement experiment in large working area. According to the requirement of uniform collimation illumination within 1 square decimeter, the layout structure with the same aperture as the imaging measurement system is adopted, and Kohler illumination is used as the basic form. Firstly, the light emitted by the light source is radiated in all directions uniformly,

OSA CONTINUUM

and then projected to the target area through the collimating lens group. Lighting requirements are as follows: in the working area of 100mm×100mm, the angle between incident light and normal is less than 1 degree, the lighting unevenness is less than 5%, and the irradiation intensity should be greater than $60W/m^2$.

2. Design scheme

In this design scheme, the whole illumination system is divided into two basic parts, namely, "homogenizing optical cavity" and "collimating optical cavity". The two parts are arranged in series, which are connected by the transition interface, and finally the illumination light is projected to the target illumination surface(Part 3). The arrangement scheme is shown in the Fig. 3 below.

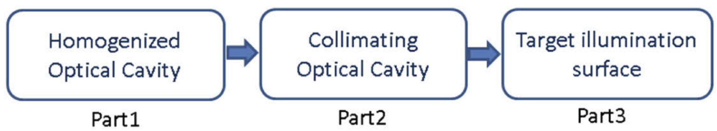

Fig. 3. Layout drawing of dual-cavity lighting system

In the design process of "collimating optical cavity", this paper proposes to adopt the structure of inverse telephoto imaging system, and set the illumination working surface at the entrance pupil of the imaging system, which coincides with the aperture stop and is located in the object space; By setting the illumination source at the image plane of the imaging system, it can be proved by Fourier optical theory that this optical structure can obtain uniform illumination effect.

The microlens array is used in the design of "homogenizing optical cavity", and the influences of two different structural forms on illumination intensity are discussed: the first one is the scheme of "collimating illumination light + double microlens array", in which the light emitted by filament is preliminarily collimated by parabolic reflector, then homogenized by double microlens array, and then converged into the collimating optical cavity by collecting lens, and the structural diagram of this scheme is shown in Fig. 4; Another form is the scheme of "light equalization with double microlens arrays at the second focus", in which an ellipsoidal mirror is adopted, and the light emitted from the filament is first converged to the second focus through the ellipsoidal mirror, and a microlens array is placed at the entrance area of the collimating optical cavity, so that the light incident to the collimating optical cavity can be uniformly angled. The structural diagram of this scheme is shown in Fig. 5.

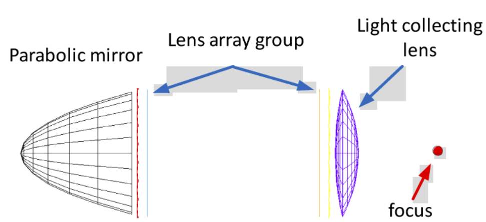

Fig. 4. Schematic diagram of "collimating illumination light + double microlens array"

Considering the collimation, uniformity and energy efficiency of lighting system, the following quantitative assessment indexes and basic design principles are defined when designing lighting system:

OSA CONTINUUM

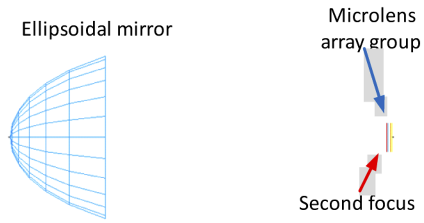

Fig. 5. Schematic diagram of "second focus double microlens array light sharing"

1. In order to improve the energy utilization rate of optical system, the ratio of the energy on the lighting working face to the total radiant energy of filament light source is taken as the evaluation function.
2. The verticality of illumination light is evaluated by the arctangent value of the ratio of the radius of the secondary light source surface to the focal length of the secondary projection system.
3. The ratio of RMS value of energy fluctuation and average energy of lighting working face is used as the standard to measure lighting uniformity.
4. Minimize the number of optical elements in the lighting system, and then reduce the energy loss on the working surface.

3. Design results

3.1. Theoretical analysis of the collimated uniform illumination system

The design of the collimating lens group applies the Fourier transform principle of the lens, and the aperture stop of the imaging system can be regarded as a uniform illumination plane. Therefore, the collimating illumination system can be regarded as an inverted system of the imaging system. That is, the working illumination surface of the collimating uniform illumination lens group is designed as the aperture diaphragm surface of the imaging system, and the illumination surface of the collimating uniform illumination lens group is designed as the image surface of the imaging system, which can greatly simplify the design complexity of the system. According to the above principles, we use CODE V as an optimization tool to optimize the above collimation lighting system in reverse order.

The relationship between the imaging lens group and the illumination lens group is inverted. We calculate the energy distribution between the entrance pupil and the image plane of the imaging lens group. The lens group is regarded as a single lens system, and its geometric relationship can be expressed as shown in Fig. 6. X_0y_0 plane is the entrance pupil plane of the imaging lens group and the aperture stop plane of the system, and x_fy_f plane is the image plane of the imaging lens group. The distance between x_0y_0 plane and the front surface of the equivalent lens is set as d_0, and the focal length of the equivalent lens group is f. The light field distribution at the aperture stop has a similar Fourier transform relationship with the light field distribution at the focal plane, and its formula can be expressed as the following formula [21] [22]:

$$\tilde{E}(x_f, y_f) = \frac{1}{i\lambda f}exp[\frac{ik}{2f}(1-\frac{d_0}{f})(x_f{}^2+y_f{}^2)]F\{\tilde{E}(x_0,y_0)\}_{u=\frac{x_f}{\lambda f},v=\frac{y_f}{\lambda f}} \tag{1}$$

The first half of the above formula can be regarded as the transmission function of the equivalent lens group:

$$\tilde{t}(x_f, y_f) = \frac{1}{i\lambda f}exp[\frac{ik}{2f}(1-\frac{d_0}{f})(x_f{}^2+y_f{}^2)] \tag{2}$$

OSA CONTINUUM

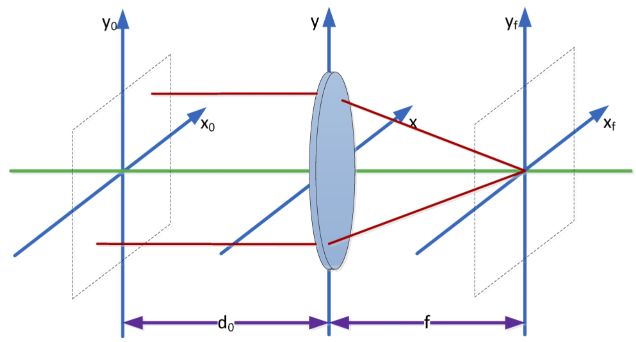

Fig. 6. Relationship between working surface and focal plane of collimating lens group

In x_0y_0 plane, the target intensity distribution in the working interval can be defined as a pupil function P(x,y):

$$P(x_0, y_0) = \begin{cases} 1, (-\frac{1}{2}a<x_0<\frac{1}{2}a, -\frac{1}{2}b<y_0<\frac{1}{2}b) \\ 0, (other) \end{cases} \tag{3}$$

Among them, a and b are the boundaries of the target square illumination area. In this paper, a = b=100mm. The ideal state of the incident light passing through the pupil function is a plane wave, so that:

$$\tilde{E}(x_0, y_0) = P(x_0, y_0) \tag{4}$$

According to formulas (1)~(4), the energy distribution on the focal plane of the designed inverse illumination system can be understood as Fourier transform of pupil function multiplied by a transmission function (phase factor related to d0), namely:

$$\tilde{E}(x_f, y_f) = \tilde{t}(x_f, y_f) \cdot F\{P(x_0, y_0)\}_{u=\frac{x_f}{\lambda f}, v=\frac{y_f}{\lambda f}} \tag{5}$$

It can be seen that the energy distribution at the plane of aperture stop x0y0 and the image plane x_fy_f are Fourier transform relations. According to the principle of light path reversibility, the spherical wave emitted from x_fy_f surface will form a uniform illumination field at the aperture stop after passing through the collimating illumination optical system. If x_fy_f surface is a point source, due to the ideal Fourier transformation of a single point pulse function into a plane, a uniform illumination field will be formed on the x_0y_0 plane in the spatial domain, which shows that the spherical wave emitted from each point at x_fy_f will form a uniform illumination field on the x_0y_0 plane. Therefore, the light intensity of the working surface η is equal to the integral of the direct current component generated by the spherical wave emitted point by point in the ε interval of x_fy_f plane. Since the illumination intensity of each point is approximately uniform, the illumination effect of the light emitted by all illumination points in the η region is nearly uniform. Therefore, this design scheme is feasible in principle.

3.2. Design of the collimating optical cavity

The function of collimating optical cavity is to generate the illumination working light source which is close to vertical illumination. In order to reduce the length of the system, TELEPHOTO structure is adopted. Because the system is not used for imaging, the original double gluing front group is replaced by a single lens. High collimation means low divergence angle. In this design, the θ maximum divergence angle θ_{max} is set to 0.5 degree(better than the requirement), and the focal length f_{lens} of the illumination system is set to 1100 mm. Therefore, the aperture stop radius

OSA CONTINUUM

rapture can be expressed as: $r_{apture} = f_{lens} \times \tan\theta_{\max}$, r_{apture}=9.6mm can be calculated, and r_{apture} is also the exit pupil radius of the homogenized optical cavity.

Because of the Fourier transform relationship between the working surface and the illumination surface, the working surface has natural and uniform characteristics, and the overall illumination characteristics will be analyzed after the system integration, so we mainly consider the focal length f_{lens} and field of view θ_{max} when designing the collimation subsystem. In addition, we consider ensuring the performance of the lighting system and the subsequent mechanical assembly requirements. The design specifications are as follows: (1) The total focal length of the lighting system is 1100 mm; (2) The half field angle is less than 1 degree; (3) Try to minimize the total volume, and the total length of the system should be less than the focal length value of 1100 mm.

CODE V software is used to design the alignment lens, which includes at least three optical elements: beam splitter prism, TELEPHOTO front mirror group and TELEPHOTO rear mirror group. In order to simplify the lighting system and improve the energy utilization rate of the system, the TELEPHOTO front lens group is changed from the original double gluing form to the single convex form, and the rear lens group is composed of a concave lens.

In the design process, we take the focal length of the system as the main specific constrain, and at the same time take the total length of the system, the thickness of components and the spacing as auxiliary constraints. As a lighting system, its MTF requirements are not high. We only need to ensure that the spatial frequency transfer function matches the spatial frequency of the microlens. The micro-element size of the microlens is 1 mm. Here, we design the first cut-off of the collimating lighting system to be higher than 1 cycle/mm. At last the focal length of the system is 1100mm, and the actual total length from the working illumination surface to the secondary illumination surface is 745.2mm, which effectively shortens the overall size of the system. The maximum incident angle at the image plane is 4.15 degrees.

The specific design structures are sown in as Table 1, and design results are sown in Fig. 7 to Fig. 9. In Fig. 8, the size of the dispersion prism looks much larger than 110 mm because it is a diagonal size.

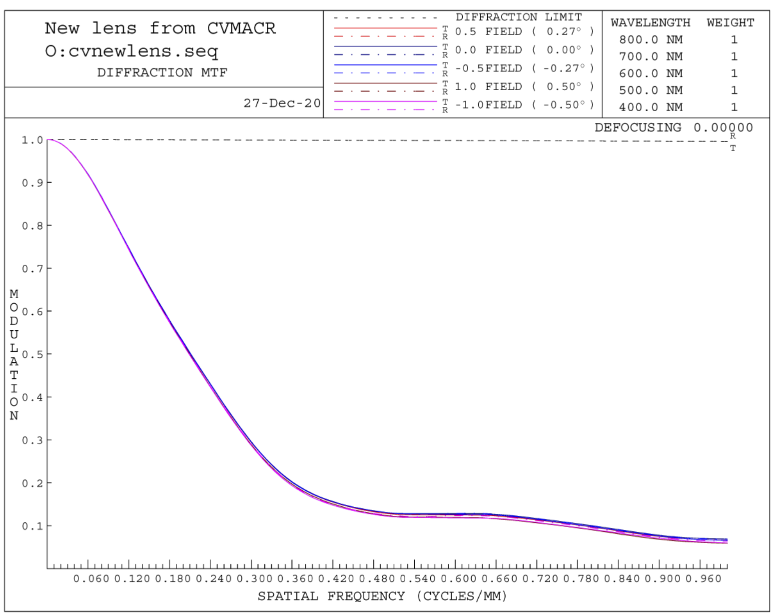

Fig. 7. Diffraction MTF of collimating optical cavity

OSA CONTINUUM

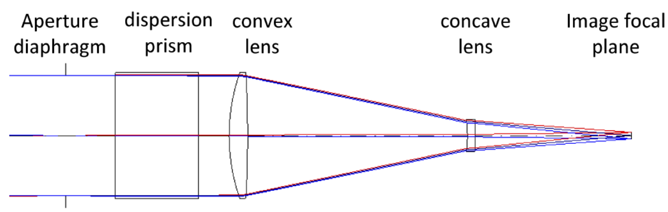

Fig. 8. Optical system structure of collimating optical cavity

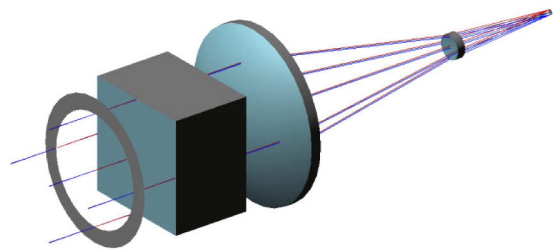

Fig. 9. Three-dimensional structure diagram of collimating illumination system

Table 1. Parameter list of optical system of collimating optical cavity

Component name	Material	Radius (mm) front surface	Back surface	Thickness (mm)	Outer diameter shape and size (mm)
dispersion prism	NBK7	Infinity	Infinity	110	Square: 110×110
convex lens	K9_CHINA	243.4	-1479.0	24.4	Circular: φ158
concave lens	HZF6_CDGM	-124.3	Infinity	10	Circular: φ39.4
image focal plane (transition interface)	/	/	/	/	Circular: φ19.2

3.3. Design of the homogenized optical cavity

The function of the homogenizing optical cavity is to generate energy radiation with uniform directions at the transition interface of the illumination system, which can be approximated as a plurality of point light sources emitting spherical waves. There are two important indexes here: one is that the energy radiation is uniform in all directions of the spatial solid angle, and the other is that the energy utilization rate of the system is high. In the design of this paper, modeling analysis is carried out in two structural forms.

3.3.1. Representation of conical reflecting surface

Any conic surface can be written as sag equation:

$$z = sag(\rho) = \frac{\frac{\rho^2}{r}}{1 + \sqrt{1 - (1+k)(\frac{\rho}{r})^2}} \tag{6}$$

ρ stands for diameter coordinates $\sqrt{x^2 + y^2}$;

r is the reference curvature radius of the curved surface;

Z is the rise of curved surface (height in Z axis direction);

OSA CONTINUUM

K is the conic constant. (k=0 is a sphere; -1 < k < 0 is an ellipsoid; K=-1 is a paraboloid; K <-1 is hyperboloid).

With microlens array, the uniform modulation of spatial divergence angle of filament radiation light can be realized by taking conical curved surface as ellipsoid or paraboloid. The conventional usage of microlens array is realized by two microlens arrays working together, but their placement positions in the above two optical path structures are different.

3.3.2. Structure form of the ellipsoidal reflection system

In the ellipsoidal structure, the ellipsoidal surface has its unique optical characteristics: the mirror has two focuses, and the light emitted from one focus will converge at the other. Therefore, if the tungsten halogen lamp is regarded as a point light source and placed at one focus of the ellipsoid, a strong light energy convergence effect will be produced at the other focus, and the simulation effect is shown in Fig. 10. We put the spiral filament instead of the point light source as the light-emitting source at the first focus, and the light emitted by the spiral filament will be concentrated near the second focus. The parameters of the spiral filament are as follows: the length of the filament cylinder is 6 mm, the diameter of the cylinder is 3 mm, the filament is wound 6 times, and the diameter of the filament is 1 mm. A microlens group is added near the second focus to homogenize the energy of the spatial divergence angle. The simulation effect diagram is shown in Fig. 11.

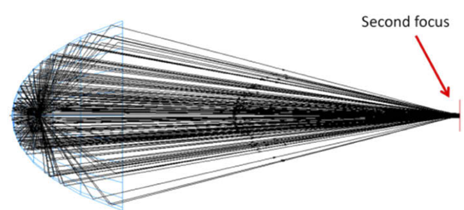

Fig. 10. Simulation diagram of illumination effect of the second focus of ellipsoidal mirror

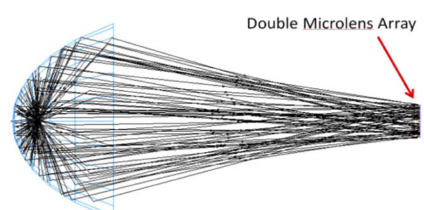

Fig. 11. A microlens array is added near the second focus of the ellipsoidal mirror optical path

3.3.3. Structure form of the parabolic reflection system

In paraboloid structure, paraboloid has its unique optical characteristics: the light emitted from the middle point between focus and vertex will be parallel to the symmetry axis after being reflected by paraboloid mirror. Therefore, when the point light source is placed at the midpoint between the vertex of paraboloid and the focus, the emitted light will be parallel to the optical axis after reflection, and will converge at the focus after passing through the light collecting lens, as shown in Fig. 12. In this optical system, the spiral filament is placed between the vertex and focus of paraboloid, microlens arrays are added in parallel light, and then the spatial divergence angle is uniformly modulated. The simulation effect diagram is shown in Fig. 13.

OSA CONTINUUM

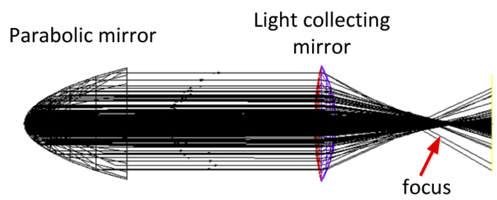

Fig. 12. Simulation diagram of lighting effect of parabolic reflector and collector mirror

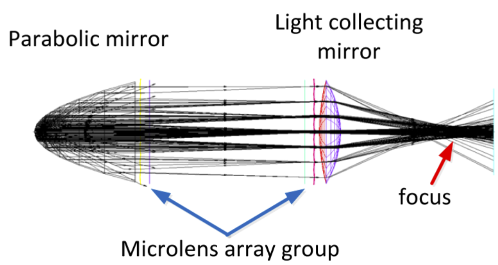

Fig. 13. The simulation diagram of microlens array is added to the parallel light path of parabolic optical system

3.3.4. Selection of mirrors

Energy matching should be considered in the selection of ellipsoidal mirror and parabolic mirror. It is difficult to convert a point light source into a flat-topped collimated beam, and the energy utilization rate of the system is very low. The reflector is the first device of the whole illumination system. In order to achieve higher energy utilization rate, the Etendue of the first device should be consistent with that of the back end as much as possible.

Parameter positioning definition of ellipsoidal reflector is shown in Fig. 14:

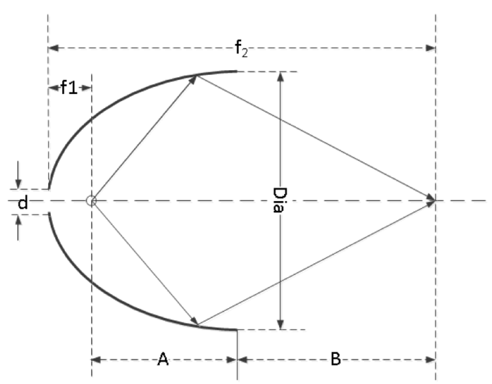

Fig. 14. Parameter definition diagram of ellipsoidal mirror

We select ellipsoidal mirrors with diameters similar to the area of the illumination surface, and try to increase the second focal length to ensure that the system has a small edge Etendue, so as to better match with the rear optical system. In the optimization link, we chose the conic surface radius, light source position, microlens array position and other parameters as optimization objects, and chose Downhill Simplex Method as optimization algorithm, so as to obtain the local optimal solution. Based on the above factors, we select the parameters of ellipsoidal mirror as shown in Table 2.

OSA CONTINUUM

Table 2. Parameter list of ellipsoidal mirror

Diameter Dia(mm)	focal length f1(mm)	focal length f2(mm)	Back hole sized(mm)	Height H(mm)	A (mm)	B (mm)
115	17	272	26	54	36	219

Parameter definition of parabolic mirror is shown in Fig. 15:

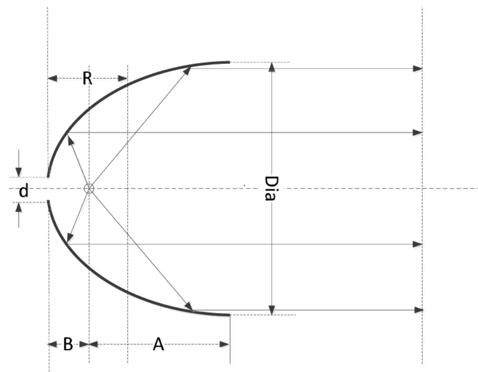

Fig. 15. Parabolic mirror parameter definition diagram

We select a parabolic reflector with a diameter similar to the size of the illumination area, and the filament position is suitable for physical installation. In the optimization link, we chose the conic surface radius, light source position as optimization objects, and chose Downhill Simplex Method as optimization algorithm, so as to obtain the local optimal solution. Based on the above factors, we select the parameters of the parabolic reflector as shown in Table 3.

Table 3. Parabolic reflector parameter table

Diameter Dia(mm)	focal length R	Back hole d(mm)	Height H(mm)	A (mm)	B (mm)
115	16	26	105	97	8

3.4. Selection of the uniform lens array group

3.4.1. Selection of the lens array for the ellipsoidal reflection system

The secondary illumination surface (transition interface) is located between the collimator lens group and the ellipsoidal condenser lens group. The secondary illumination surface is equivalent to the light source surface of the collimator lens group, and the angle uniformity of its outgoing light determines the illumination uniformity of the target illumination surface. Therefore, it is necessary to add an angle light equalizing element at this position to realize the uniformity of the light intensity at the exit angle. The microlens array has the function of discretizing the exit angle of incident light. When parallel light is incident on the microlens array, the propagation direction of the emergent light fills the numerical aperture space of the microlens group. Scattering effect on parallel light is shown in Fig. 16.

The illumination target area is 110mm×110mm, the side length of the illumination area is expressed by D_{area}, and the size of the secondary illumination surface is a circular area with a diameter of 19.2 mm. The focal length/unit size ratio of the microlens array designed by us is the

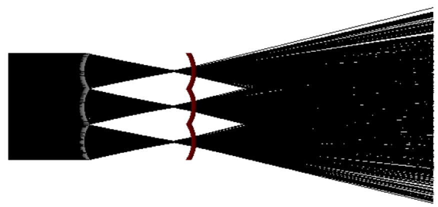

Fig. 16. Scattering effect diagram of parallel light by microlens

same as the F number of the collimating system, so the following formula can be obtained:

$$\frac{f_{array}}{a_{array}} = \frac{f_{lens}}{D_{area}} = \frac{1100mm}{110mm} = 10 \tag{7}$$

Therefore, it is necessary to select microlens array elements whose ratio of cell focal length to cell side length is around 10. In this experiment, we selected two microlens arrays made of SILICA with focal length of 10mm and side length of 1mm. The detailed data is shown in Table 4:

Table 4. Parameter table of microlens array in ellipsoidal reflection system

Parameter	Side length D(mm)	Number of rows	Number of columns	Micro side length (mm)	Focal length (mm)	Material	Thickness (mm)
Value	20	20	20	1	10	Silica	1

3.4.2. Selection of the lens array for parabolic reflection system

In parabolic averaging system, the lens array needs to be placed in parallel light path after the previous analysis. However, compared with ellipsoidal reflection system, the parallel system has a huge optical aperture, which reaches 115mm. At this size, the microlens array can no longer be used, and the smalllens array should be used. At the same time, the beam divergence caused by adding lens array should be considered in the design process. We still set the ratio of focal length and unit size to be the same as the F number of the collimating system (equal to 10), and optimize the design of the collecting mirror to find a balance between the beam divergence angle and the energy concentration. Considering these factors comprehensively, the lens array parameters of the parabolic reflection system are shown in Table 5.

Table 5. Parameter table of microlens array in parabolic reflection system

Parameter	Side length D(mm)	Number of rows	Number of columns	Micro side length (mm)	Focal length (mm)	Material	Thickness (mm)
Value	122.5	7	7	17.5	175	Silica	10

3.5. Analysis of the comprehensive ability of the lighting system

3.5.1. Comprehensive capability analysis of the ellipsoidal reflection system

The ellipsoidal reflective illumination system model is established by using the simulation software ASAP, and the two-dimensional distribution of the system is shown in Fig. 17; We traced 25 million rays with software. At the target position, we placed a 100mm×100mm detector to receive the light energy, and used the spiral luminous filament instead of tungsten halogen lamp as the light source.

OSA CONTINUUM

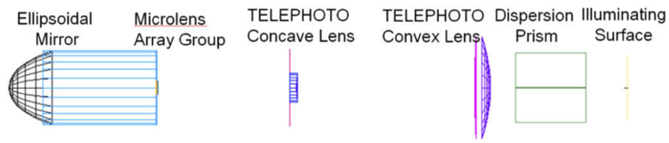

Fig. 17. Layout of Integrated Lighting System for Ellipsoidal Reflection System

The energy radiation power was 250W. The tracing process diagram is shown in Fig. 18. The light spot distribution map on the lighting working face is shown in Fig. 19, and the overall visible energy distribution is uniform. However, due to the large lighting area, the limited total number of simulated light rays and other factors, there is not enough light to fill the whole lighting face, so the density of the obtained lighting spot map is insufficient, but the uniformity of energy distribution can be seen intuitively.

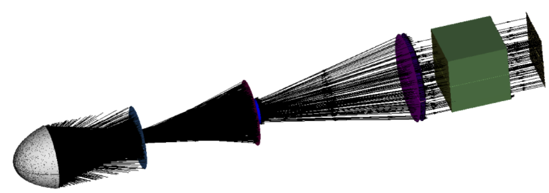

Fig. 18. Analysis of illumination light propagation in ellipsoidal reflection system

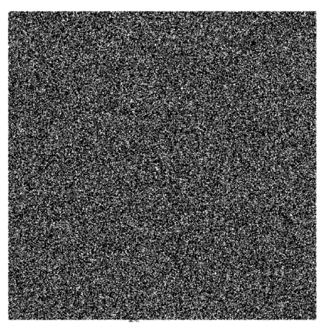

Fig. 19. Light spot distribution in 100mm×100 mm working face of ellipsoidal reflection system

Statistical analysis is carried out on the above energy distribution, and the 100mm×100mm area is divided into 16×16 sub-areas, and the energy distribution in each grid area is counted. As shown in Fig. 20, the value represented by color is between 0.4335662E-03 and 0.5216284E-03, which shows that the overall uniformity is better. The final statistics are shown in Table 6:

Unevenness η of system energy distribution is defined as energy jitter divided by average energy, which can be expressed as the following formula:

$$\eta = \frac{RMS_{var}}{Average} = \frac{0.1328541E-04}{0.4750857E-03} = 2.80\% \tag{9}$$

It can be seen that the illumination unevenness of the system is 2.80%, which meets the index requirement that the illumination unevenness is less than 5%, we can calculate that the energy

OSA CONTINUUM

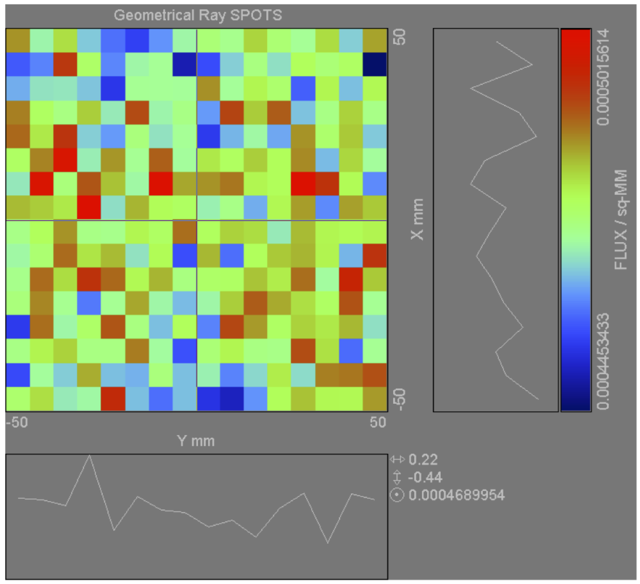

Fig. 20. Energy distribution of 100mm×100 mm working face of ellipsoidal reflection system

Table 6. 100mm×100mm energy distribution statistical data sheet

Area: 100mm×100mm					
Statistics on 16 by 16 data set					
FLUX / sq-MM		Location		Y mm	X mm
Minimum	0.4453433E-03	15	16	40.62490	46.87476
Maximum	0.5015614E-03	9	4	3.124953	-28.12494
Average	0.4749798E-03	8	9	-3.125037	3.124934
RMS var	0.9907153E-05	4	5	27.45272	29.27882
TOTAL FLUX = 4.749772W (475W/m^2)					

utilization rate of the system is 1.90%. Considering that the photoelectric conversion efficiency of filament light source is about 30% (most energy is lost in the form of heat) and the reflectivity of ellipsoidal mirror is about 86%, we can get that the actual photoelectric point conversion efficiency is about 0.49%(122.5W/m^2), which is very close to the energy utilization rate of 0.5% obtained in Dr. Lv Tao's thesis(page56) [23]. Although Dr. Lv Tao's thesis is inconsistent with the application scenarios pursued in this paper, the light sources used are inconsistent, and the complexity of the system is also inconsistent, but the energy utilization efficiency has certain reference. The difference is that this paper mainly relies on model analysis, while Dr. Lv Tao's thesis is mainly based on practical experience.

In the analysis of alignment, we first select 818 rays that hit the target surface for analysis, and these rays are distributed in all target positions; Secondly, the angle data between light and optical axis is obtained one by one. Within the maximum incident angle, it is divided into 21 parts at equal intervals; At last, using the method of mathematical statistics, the distribution interval of incident angle is counted, the probability distribution diagram of "normalized probability - incident angle" is drawn, and the graph is compared with the normal distribution curve. The ordinate represents the normalized probability distribution, and the abscissa represents the angle

OSA CONTINUUM

between the incident ray and the normal. It is found that the angle of incident light on the working surface is in the range of 0 degree to 1 degree, which obeys the normal distribution with the center of 0.5 degree. As shown in the Fig. 21. The incident rays on the working surface are not normally distributed around 0 degrees. This result is not perfect, but it can meet the demand. However, according to our preliminary analysis, it may be because the microlens array has not completely eliminated the ring effect of ellipsoidal mirror, and this work needs further analysis.

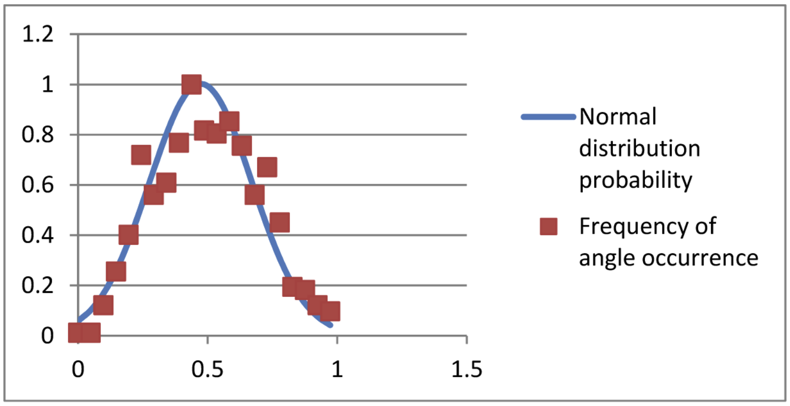

Fig. 21. Probability distribution diagram of collimation degree of ellipsoidal reflection system

3.5.2. Comprehensive capability analysis of the parabolic reflection system

We use the simulation software ASAP to build a parabolic reflective lighting system model, and the two-dimensional distribution of the system is shown in Fig. 22; We traced 25 million rays with software. At the target position, we placed a 100mm×100mm detector to receive the light energy, and used the spiral luminous filament instead of tungsten halogen lamp as the light source. The energy radiation power was 250W. The tracing process diagram is shown in Fig. 23. The light spot distribution map on the lighting working face is shown in Fig. 24.

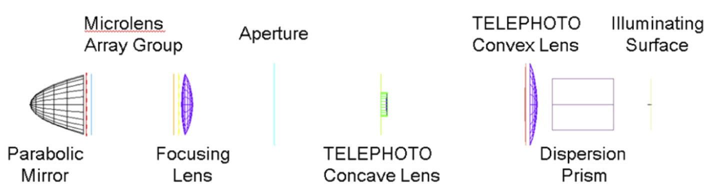

Fig. 22. Layout of Integrated Lighting System for Parabolic Reflection System

Fig. 23. Analysis of Illumination Light Propagation in Parabolic Reflection System

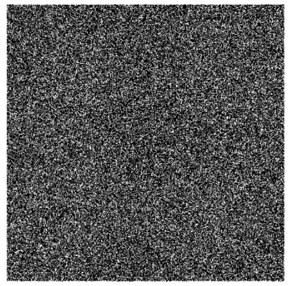

Fig. 24. The light spot distribution of 100mm×100 mm working face of parabolic reflector system

Statistical analysis is carried out on the above energy distribution, and the 100mm×100mm area is divided into 16×16 sub-areas, and the energy distribution in each grid area is counted, as shown in Fig. 25, from the value represented by color between 0.2912403E-03 and 0.3748518E-03. The final statistics are shown in Table 7:

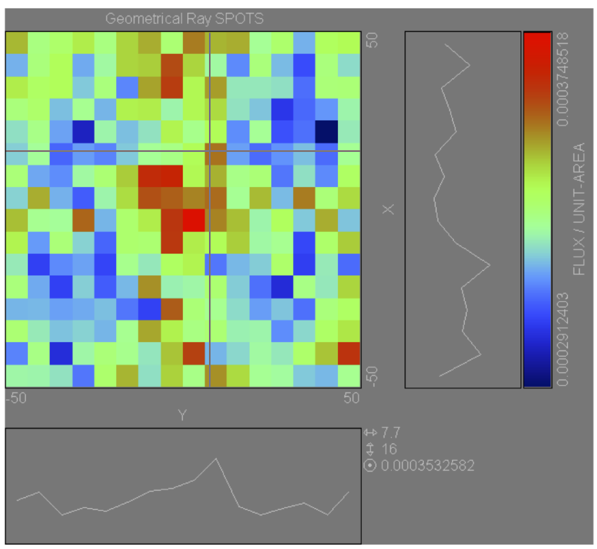

Fig. 25. Energy distribution of 100mm×100 mm working face of parabolic reflection system

Table 7. 100mm×100mm energy distribution statistical data sheet

Area:100mm×100mm					
Statistics on 16 by 16 data set					
FLUX / sq-MM		Location		Y mm	X mm
Minimum	0.2912403E-03	12	15	21.87498	40.62448
Maximum	0.3748518E-03	8	9	-3.124813	3.124830
Average	0.3300097E-03	9	9	3.125134	3.124830
RMS var	0.1345530E-04	5	4	29.07974	27.76058
TOTAL FLUX = 3.300039W (330W/m^2)					

OSA CONTINUUM

The energy distribution unevenness η of the system can be expressed as the following formula:

$$\eta = \frac{RMS_{var}}{Average} = \frac{0.1345530E^{-04}}{0.3300097E^{-03}} = 4.08\% \tag{10}$$

It can be seen that the illumination unevenness of the system is 4.08%, which meets the index requirement that the illumination unevenness is less than 5%, and the energy utilization rate of the system is 1.32%. Considering that the photoelectric conversion efficiency of filament light source is about 30% (most energy is lost in the form of heat) and the reflectivity of ellipsoidal mirror is about 86%, we can get that the actual photoelectric point conversion efficiency is about 0.34%(85W/m^2).

In the analysis of alignment, we select 931 rays that hit the target surface for analysis, and we use the same analysis method as ellipsoidal reflector. It can be found that the incident angle of the working surface is partly larger than 1 degree, and the center of gravity of the incident angle is also larger than 0.5 degree. As shown in the Fig. 26. The ordinate represents the normalized probability distribution, and the abscissa represents the angle between the incident ray and the normal. On the whole, the collimation degree of parabolic reflection system is inferior to that of ellipsoidal reflection system.

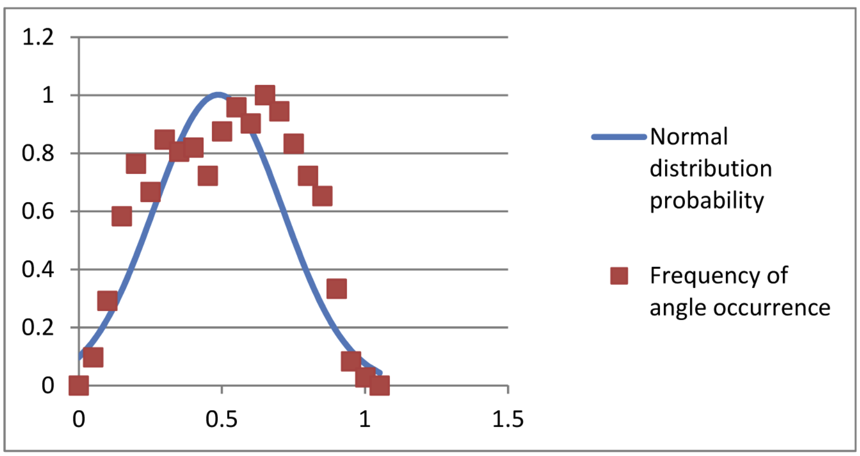

Fig. 26. Probability distribution diagram of collimation degree of parabolic reflection system

4. Analysis

The following two schemes are compared from the aspects of energy uniformity, volume, complexity, energy utilization rate and so on:

1. It is easy to find from the energy distribution diagram that the illumination effect caused by parabolic reflector structure is not uniform enough. Peak-like distribution structure with strong middle energy and low surrounding energy is produced in the detector, as shown in Fig. 23. One of the reasons is that there is a condenser lens between the lens array and the transition interface, which breaks the uniform light effect of the microlens to a certain extent. However, the ellipsoidal reflector lighting structure has better performance in energy uniformity.

OSA CONTINUUM

2. In terms of the length of illumination system, the optical length of parabolic reflection system is 1217mm, and the length of ellipsoidal reflection system is 1067 mm. Obviously, ellipsoidal reflection system has advantages because the lens array of parabolic system has a longer focal length and occupies a longer space, which makes the illumination system occupy more space.
3. From the number of unit devices, the ellipsoidal reflection system has fewer devices.
4. From the energy utilization rate, the energy utilization rate of ellipsoidal reflection system is about 0.49%, and that of parabolic emission system is 0.34%. Obviously, ellipsoidal reflection system has more advantages. The energy utilization rate of these two systems is relatively low, which is mainly determined by the collimation requirements of the illumination beam. Under the constraint of high collimation, the etendue of the illumination surface is much smaller than that of the light collection system.
5. The lighting system is a projection system with fixed energy ratio, so if we want to increase the illuminance of the target working surface, we can consider replacing the lighting source with higher power, such as xenon lamp.
6. This paper focuses on the analysis of system composition and index accessibility, but it is worth noting that the aberration of collimation system, polynomial coefficient of reflection surface of homogenization system, relative position of aperture diaphragm and other factors will have an impact on lighting effect, which should be carried out in the follow-up work.

5. Conclusion

Based on the basic form of Kohler illumination and the basic structure of “collimating optical cavity” and “homogenizing optical cavity”, we designed a high uniformity and high collimation illumination system for near-field measurement. Based on Fourier energy propagation theory, it is proved that it is reasonable to set the secondary illumination plane at the image plane of TELEPHOTO system. At the same time, starting from the actual lighting effect, we use simulation software to simulate the parabolic reflector lighting system and ellipsoidal reflector lighting system, and through comparative analysis, we determine that ellipsoidal reflector has superior performance. In the working area of 100mm×100mm, the quasi-right angle of illumination of ellipsoidal reflection system is about 0.5, and the illumination unevenness is about 2.80%, which is less than or equal to the theoretical requirement; The radiation power of the irradiated surface is 4.75W, which meets the index requirements.

However, there is still the problem of system etendue mismatch, resulting in energy loss. In the follow-up work, we will focus on how to improve the system energy utilization rate.

Funding. Department of Science and Technology of Jilin Province (20180201039GX); Chinese Academy of Sciences (YJKYYQ20190083); National Natural Science Foundation of China (61905242); Chinese Academy of Sciences (CXJJ-20S04).

Disclosures. The authors declare no conflicts of interest.

References

1. C. Hammond and J. Heath, “Symmetrical ray diagrams of the optical path ways in light microscopes,” Microscopy and Analysis **115**, 5–8 (2006).
2. S. Chenghua, W. Shengjie, X. Danyang, and D. C. Han Yonghao, “Design and implementation of slit lamp microscope illumination system,” Advances in Laser and Optoelectronics **11**, 358–363 (2017).
3. C. Chai, H. Yan, J. Luo, Z. Chi, H. Lin, and L. Xiaojun, “Design and simulation of structured light illumination microscope illumination system,” *Tool Technology* 7, (2019).
4. X. Hongbo, J. Min, Y. Lei, M. Qingbin, and F. Chunbin, “Design of long-distance uniform lighting system with a single LED,” J. Appl. Opt. **38**, 543–548 (2017).
5. Z. Dengchen and W. Xiying, “Design of illumination system for microscope with high magnification and large depth of field,” Optical Instruments **04**, 4–10 (1982).

OSA CONTINUUM

6. H J Levinson, *Principles of lithography* (SPIE Press, 2010), pp. 162–200.
7. C. Weilin, Z. Fang, L. Dongliang, Z. Aijun, Y. Baoxi, and H. Huijie, “Research on high-precision correction method of illumination light field uniformity of lithography machine,” Acta Opt. Sin. **38**(7), 0722001 (2018)..
8. J. Jiahua, L. Yanqiu, S. Shihuan, and M. Shanshan, “Design of a high-numerical-aperture extreme ultraviolet lithography illumination system,” Appl. Opt. **57**, 20 (2018).
9. M. Long, L. Yi, P. Xin, H. Yanmin, and S. Fengming, “Scaled SFS method for Lambertian surface 3D measurement under point source lighting,” Opt. Express **26**(11), 14251–14258 (2018).
10. A. Correia, P. Hanselaer, and Y. Meuret, “Improving the opto-thermal performance of transmissive laser-based white light sources through beam shaping,” Opt. Express **27**(8), A235–A244 (2019).
11. Y. Ding and G. Peifu, “Free-form reflector for uniform illumination,” Acta Opt. Sin. **27**, 540–544 (2007).
12. F. Hanyi and L. Yuanyuan, “High uniformity small aperture laser illumination system,” Chinese Journal of Liquid Crystals and Displays **33**(7), 13–19 (2018).
13. C. Hu, Y. Hu, and H. Wang, “Laser illuminator for low-light-level observation and aiming system,” J. Appl. Opt. **3**, 5–8 (2001).
14. M. Yayun, H. Shaokun, Z. Yu, and H. Fuming, “A laser illumination method based on fiber array,” Optical Technology **44**(002), 201–205 (2018).
15. K. Creath and G. Goldstein, “Processing and improvements in dynamic quantitative phase microscope,” Proc. SPIE **8589**(13), 1672–1675 (2013).
16. I. Avner Safrani, “Real-time phase shift interference microscopy,” Opt. Lett. **39**(17), 5220–5223 (2014).
17. A. Safrani and I. Abdulhalim, “High-speed 3D imaging using two-wavelength parallel-phase-shift interferometry,” Opt. Lett. **40**(20), 4651 (2015).
18. D. Arnaud, “Extended Full-field Optical Coherence Microscopy,” AIP Conf. Proc. **1537**, 123 (2013).
19. Zhang Jinkai, Research on the Measurement Method of Variable Field of View Structured Light Microscopic Stereo Vision for Mesoscale Parts.
20. Song Yun Cen, Research on Basic Algorithm of PCB Automatic Optical Inspection System.
21. Lv Naiguang, Fourier Optics (Mechanical Industry Press, 2006).
22. Ji Jiarong, Advanced Optics Course (Science Press, 2007).
23. Lv Tao, Study on solar simulation technology with high collimation and high irradiation intensity. 2014.